Journal of the European Ceramic Society 22 (2002) 1927–1936

www.elsevier.com/locate/jeurceramsoc

Processing and mechanical properties of Al_2O_3–5 vol.% Cr nanocomposites

Y. Ji[1], J.A. Yeomans*

School of Engineering, University of Surrey, Guildford, Surrey, GU2 7XH, UK

Received 3 August 2001; received in revised form 19 November 2001; accepted 8 December 2001

Abstract

The use of chromium (III) acetylacetonate as a source of nanometre sized chromium particles for the production of Al_2O_3–5 vol.% Cr nanocomposites has been investigated. The details of the processing procedure are crucial in determining the mechanical properties of the composite. The highest strength and fracture toughness, 736 ± 29 MPa and 4.0 ± 0.2 MPa $m^{1/2}$, respectively, were obtained for the nanocomposite hot pressed at 1450 °C. It is shown that the strengthening in Al_2O_3–5% Cr nanocomposites mainly results from microstructure refinement in that the mean alumina matrix grain size in the optimum composite was 0.68 μm compared with a grain size of 3.6 μm in the monolithic alumina hot pressed under identical conditions. Crack bridging and crack deflection by the nano-sized Cr particles did not occur to any significant extent. The slight improvement in fracture toughness may result from the observed change in fracture mode from intergranular fracture for monolithic alumina to transgranular failure for the nanocomposites.

Keywords: Al_2O_3–Cr; Composites; Grain size; Hot pressing; Mechanical properties; Microstructure-final

1. Introduction

Alumina is a widely used ceramic due to its refractoriness, wear resistance and chemical stability. However, the brittleness of Al_2O_3 limits its potential applications. Incorporation of metallic second phases into alumina matrices has been shown to give significant improvements in fracture toughness. The maximum toughening increment is achieved when the metal particle deforms plastically and bridges the crack faces. This is easier to achieve when the second phase is in the form of a continuous network but in terms of maintaining some elevated temperature capability and electrical insulation it may be desirable to have the metallic phase in the form of discrete particles. Within the discrete particle category, there have been several reports on the effects of different metals including Ni,[1–4] Fe[5] Ag,[6] Mo[7] and FeAl.[7]

Since the early 1990s, when Niihara[8] and co-workers began to report on the beneficial effects of incorporating nanometre-sized particles in ceramic matrices to produce nanocomposites with significantly improved strengths, there has been considerable interest in making composites with much reduced particle sizes. Development of alumina-metal nanocomposites is of interest because of the potential to improve fracture strength and fracture toughness simultaneously by combining the "nanocomposite effect" with the ductility of the metallic phase. Various metals have been incorporated into alumina including Ni,[9,10] Mo,[11] W,[12,13] Fe,[14] Cr,[15] Cu[16] and NiCo.[17]

In the earlier work on alumina-metal nanocomposites the materials were produced by hot pressing powder blends that comprised either alumina and metal powders or alumina and metal oxide powders. As the hot pressing was usually in a graphite die, the metal oxide was reduced to the metal. More recent work has explored other ways of creating nanometre sized metal particles within the composite, including decomposition of oxide solid solutions to give (Fe, Cr)–Al_2O_3,[18] reactive milling of Cr_2O_3 or CrO_3 and Al to produce Al_2O_3–Cr[15] (although this method does produce a significant

* Corresponding author.
E-mail address: j.yeomans@surrey.ac.uk (J.A. Yeomans).
[1] Present address: Department of Materials, Imperial College of Science, Technology and Medicine, Prince Consort Road, London, SW7 2BP, UK.

0955-2219/02/$ - see front matter
PII: S0955-2219(01)00528-3

fraction of metallic particles in the micrometre size range), coating metal (Mo[19] and Ni[20]) particles with alumina, again producing composites with coarser metal particles, and infiltration of an alumina perform with a metal salt solution.[21] The use of metal nitrate precursors has been reported for several systems and the results of composites prepared by this route compared with those from composites made from alumina-metal oxide mixtures.[9,22,23] Composites made from the nitrate precursors have higher fractions of intergranular particles, smaller matrix grain sizes and higher strengths than similar composites made from alumina and metal oxide starting materials. One of the highest strength values reported is for an addition of 5 vol.% Ni from a nitrate precursor, which resulted in an average alumina grain size of 0.64 μm and a fracture strength of 1090 MPa, compared with a grain size of 0.96 μm and strength of ~980 MPa for a similar composite made from an alumina-nickel oxide powder and a monolithic alumina strength of 700 MPa for a 1.2 μm average grain size.[9] However, Chen and Tuan,[10] working with a pressureless sintered 5 vol.% Ni-alumina composite, also from a nitrate precursor, report a strength of 526 MPa for a matrix grain size of 0.49 μm, although their composite was not quite as dense (96.6%). In the present work, a chemical powder processing method is explored as a means of producing Al_2O_3–Cr nanocomposites.

2. Experimental procedure

2.1. Production of the powder blends and composites

The starting powders used to fabricate the Al_2O_3–Cr nanocomposites were Al_2O_3 AKP-50 powder and chromium (III) acetylacetonate (the Cr precursor). The Al_2O_3 powder was supplied by Sumitomo Chemical Co. Ltd., Tokyo, Japan. The purity of the Al_2O_3 powder is 99.99% and the particle size is in the range 100–300 nm. Chromium (III) acetylacetonate ($[CH_3COCH{=}C(CH_3)O]_3Cr$), referred to as $Cr(ACAC)_3$, with a purity of 97%, was supplied by Aldrich Chemical Company, Inc.

Appropriate amounts of Al_2O_3 and $Cr(ACAC)_3$ were weighed out to give 5 vol.% of pure chromium in the final product, assuming that all the $Cr(ACAC)_3$ precursor was reduced to metallic Cr. Attempts to ball mill a mixture of Al_2O_3 and $Cr(ACAC)_3$ in ethanol were not successful as a poor suspension was produced. In order to overcome this problem, the weighed Al_2O_3 and $Cr(ACAC)_3$ powders were ball milled in ethanol separately first using alumina cylindrical milling media. The two slurries were mixed and ball milled for another 24 h. This gave a well-dispersed suspension. The slurry was then dried in a vacuum oven at 65 °C to avoid oxidization of the organic precursor. The dried powder blend was broken down by pestle and mortar. After passing through a 53 μm sieve, the powder mixture was calcined to burn out the organic material. Calcinations in argon were carried out at 200, 350 and 400 °C to determinate an appropriate temperature such that the organic material was completely removed whilst oxidization was avoided. Some of the powder was passed through a 53 μm sieve (route I) after the calcination. The rest of the powder was ball milled again in ethanol for 24 h in order to break up the agglomerates (route II). After drying in an oven at 65 °C for 24 h, the powder blend was passed through a 53 μm sieve. Hot-pressing was used to consolidate the composites in a graphite die under argon protection. All samples were heated at 20 °C min^{-1}. For route I powder blends, a uniaxial pressure of 25 MPa was applied on reaching a temperature of 1400 °C. Both temperature and pressure were held for 30 min. For the powder blend from route II, a uniaxial pressure of 35 MPa was applied once the temperature reached 1000 °C. On reaching the sintering temperature, both temperature and pressure were held for 1 h. The pressure was then released and the system cooled down to room temperature for these two slightly different hot pressing procedures. Several pure AKP50 Al_2O_3 samples were hot pressed at different temperatures and times in order to produce monolithic materials with the same grain size as the nanocomposites. Also, for comparative purposes, an Al_2O_3–5 vol.% Cr microcomposite was fabricated. AKP50 Al_2O_3 powder and chromium powder (<5 μm) were milled in ethanol for 24 h, dried, sieved then hot pressed at 1400 °C for 30 min under 30 MPa pressure.

2.2. Microstructural characterisation

The densities of the composites were determined by Archimedes' principle. Differential scanning calorimetry (DSC) of the Al_2O_3–$Cr(ACAC)_3$ powder blend was conducted using a Stanton Redcroft (STA-780 series) thermal analyser instrument. Phase identification was performed using X-ray diffractometry (XRD) on a Philips PW1050 X-ray diffractometer. Microstructural observations of the powder blends, the polished surfaces and fracture surfaces were examined by scanning electron microscopy (SEM) and transmission electron microscopy (TEM). Thin foils for TEM investigations were prepared using standard preparation methods for ceramic materials, i.e. mechanical cutting, dimple grinding/polishing, followed by ion-beam etching. TEM studies were conducted on a Philips CM 200 microscope equipped with an energy dispersive X-ray (EDX) analyser.

The grain sizes of the monolithic Al_2O_3 and Al_2O_3–Cr composites were measured from thermally etched surfaces. The thermal etching of the hot pressed monolithic Al_2O_3 and the Al_2O_3–Cr composites was conducted at 1350 °C for 30 min in air and in argon, respectively. The grain size was measured by linear intercept method. The

Cr particle size and distribution were obtained from TEM observation of over 300 particles.

2.3. Mechanical properties determination

Indentation tests were performed using a Vickers pyramid diamond hardness testing machine (Hardness Testing Machines Ltd.). The specimens were polished to a 1 μm diamond surface finish before the tests. The load used was 196 N with a loading time of 10 s. Each indentation was placed at least ten diagonal lengths away from adjacent indentations to ensure that there was no overlap with the stress field of neighbouring indentations. The average length of radial cracks, c, emanating from the indentation corners was used to obtain a value of fracture toughness using Liang's equation.[24] The fracture toughness results were averaged over 10 indentations per specimen.

The flexure strength was evaluated using 3-point bend testing. Bars were cut from the hot pressed bulk and then ground to 2×1.5×25 mm. The machining damage was mechanically removed by polishing, ultimately to a 3 mm diamond surface finish on the tensile surface. The other three surfaces were polished to a 30 μm finish. The edges were chamfered to avoid surface defects. The 3-point bend testing was conducted on an Instron 1195 mechanical testing machine with a cross-head speed of 0.5 mm/min and a span of 20 mm. The fracture strength results were averaged over 3–4 specimens.

3. Results and discussion

3.1. The powder mixture

In order to determine an appropriate calcination procedure, DSC was conducted on the Al_2O_3–$Cr(ACAC)_3$ powder blend in air and argon atmospheres and the results were recorded as shown in Fig. 1 (a) and (b), respectively. It can be seen that powder mixtures showed different features under heat treatment in air and argon. The endothermic peaks present at 218 °C on the DSC curve in both cases correspond to the melting point of $Cr(ACAC)_3$. Decomposition occurred at about 300 °C in both cases as evidenced by the significant weight loss around this temperature. The two small exothermal peaks after 400 °C in argon (Fig. 1b) may be the result of slight oxidation. However, it is clear that significant oxidation of the powder blend was inhibited by heat treatment in argon.

Fig. 2 shows the XRD profiles from three stages of the processing. The XRD result for the densified composite is included for comparison. The XRD pattern before calcination (Fig. 2a) contains the characteristic peaks of α-Al_2O_3 and $Cr(ACAC)_3$. At heat treatment temperatures below 350 °C (Fig. 2b), peaks from $Cr(ACAC)_3$ still appear which indicate that the organic precursor has not decomposed completely. All peaks from $Cr(ACAC)_3$ disappeared after calcination at 350 °C and peaks from the Cr phase appeared (Fig. 2c). Thus, the decomposition occurs after 350 °C, which is in agreement with the DSC result. After hot pressing at 1450 °C for 60 min, the predominant peaks are from α-Al_2O_3 and Cr with a small amount of Cr_2O_3 (Fig. 2d). No carbide phase was identified by XRD. It is noted that all peaks are broad suggesting the presence of small grain sizes and/or high residual stresses.

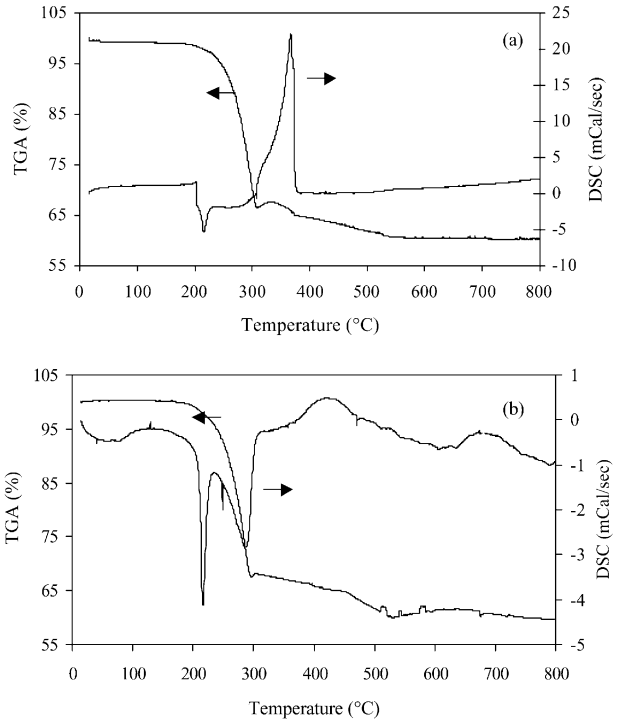

Fig. 1. DSC and TGA results for the Al_2O_3–$Cr(ACAC)_3$ powder blend heated in (a) air and (b) argon.

The powder blends before and after calcinations at 350 °C in argon were studied by TEM as shown by Fig. 3. In the starting powder, the $Cr(ACAC)_3$ particles are located on the Al_2O_3 particle surfaces. EDX analysis of the $Cr(ACAC)_3$ identified silicon and sodium as impurity elements. After calcining at 350 °C, the $Cr(ACAC)_3$ decomposed to nearly spherical particles, with sizes of about 20 nm, located on the alumina surfaces (Fig. 3b). TEM- SADP (selected area diffraction patterns) confirmed that the particles were chromium. Thus, $Cr(ACAC)_3$ can be used as a precursor for chromium particles in an alumina–chromium nanocomposite, provided that an appropriate calcination treatment, such as 350 °C in argon, is used.

3.2. Microstructural characterisation of the Al_2O_3–Cr nanocomposites

The results of the microstructural characterisation of all the samples are summarised in Table 1. As described

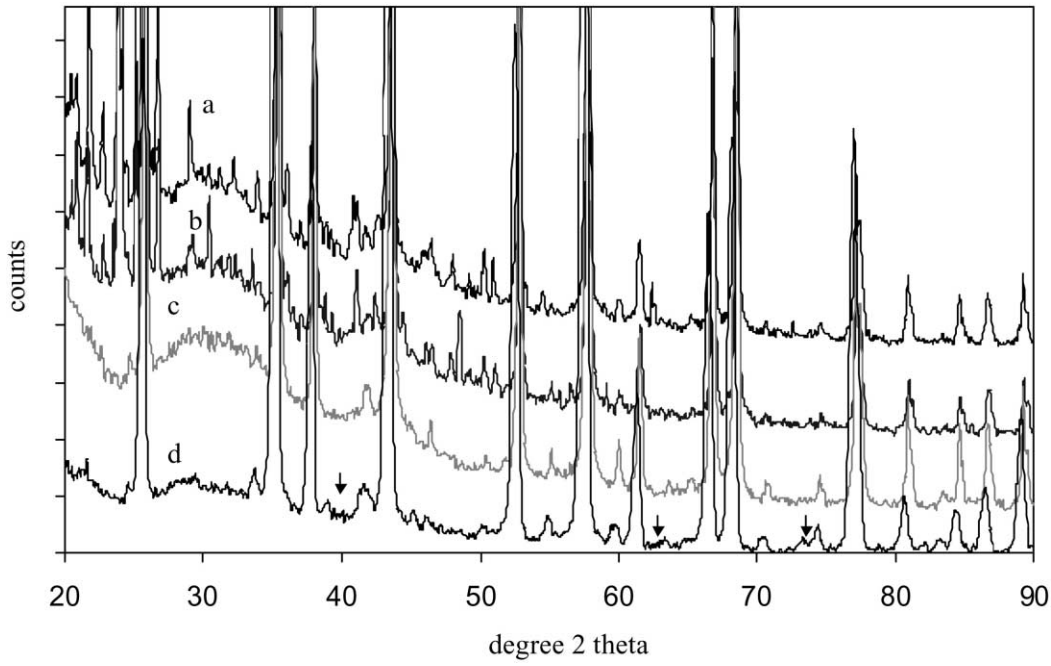

Fig. 2. XRD results for (a) the Al_2O_3–$Cr(ACAC)_3$ powder blend before calcination, (b) a powder blend calcined at 200 °C in argon, (c) a powder blend calcined at 350 °C in argon, and (d) a composite hot pressed at 1450 °C for 1 h. The positions of some of the Cr peaks are arrowed.

Table 1
Hot pressing schedules, densities and grain/particle sizes of the monolithic Al_2O_3, the Al_2O_3–5 vol.% Cr nanocomposites and the Al_2O_3–5 vol.% Cr microcomposite

	Specimen	Temperature (°C)	Time (min)	Density (mg m^{-3})	Relative density (%)	Grain size (μm)	Particle size (nm)
	Al_2O_3	1400	30	3.92	98.2	2.7	
	Al_2O_3	1450	60	3.99	99.9	3.5	
Nano, Route I	Al_2O_3–Cr	1400	30	3.81	92.0	1.3	467
Nano, Route II	Al_2O_3–Cr	1450	60	4.02	97.1	0.68	124
Nano, Route II	Al_2O_3–Cr	1500	60	4.04	97.6	0.85	
Nano, Route II	Al_2O_3–Cr	1600	60	4.06	98.1	1.6	186
Micro	Al_2O_3–Cr	1400	30	4.08	98.6	2.1	1500

in the experimental procedure, two slightly different powder processing methods were used to produce Al_2O_3–Cr nanocomposites, i.e. without (route I) or with (route II) ball milling after calcination. The Al_2O_3–Cr nanocomposite produced using route I had a low density (92% theoretical density) and an uneven chromium particle size distribution after fabrication at a relatively low hot pressing temperature, i.e. 1400 °C. Within the microstructure there were areas of high porosity that may indicate that agglomerations from powder processing inhibited the densification of the compact (Fig. 4a). Furthermore, small chromium particles with sizes less than 100 nm and bigger ones of about 1 μm co-exist with an average particle size of 467 nm. Thus, there is a conflict since higher hot pressing temperatures and longer times are needed to achieve higher density but these conditions are likely to cause enlargement of the chromium particles. Thus, it is unlikely that nanocomposites with a high density and a small particle size can be produced by route I. Breaking up the agglomerations is a crucial step in obtaining a uniform microstructure. Therefore, another powder processing route, i.e. ball milling after calcination (route II), was used to break up the agglomerations and promote an even distribution of chromium inclusions. Furthermore, a pressure of 35 MPa was applied to aid closure of the porosity once the hot pressing temperature reached 1000 °C. As expected, SEM observation of the route II Al_2O_3–Cr nanocomposite hot pressed at 1450 °C for 60 min revealed a more homogeneous distribution of Cr particles and lower porosity (Fig. 4b).

Fig. 5 shows the densification behaviour of the monolithic Al_2O_3 and the Al_2O_3–Cr nanocomposites (route II) as a function of the hot pressing temperature. For the monolithic alumina and Al_2O_3–Cr micro-composite specimens, a density above 98% theoretical density

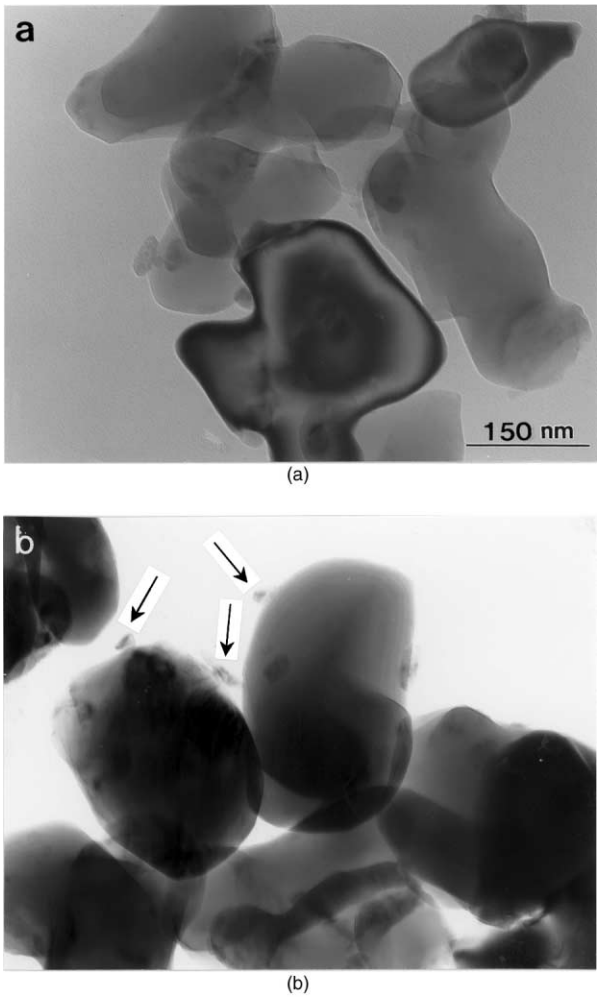

Fig. 3. TEM images of the Al_2O_3–$Cr(ACAC)_3$ powder blend (a) before calcination and (b) after calcination at 350 °C. The arrows indicate the positions of the chromium particles.

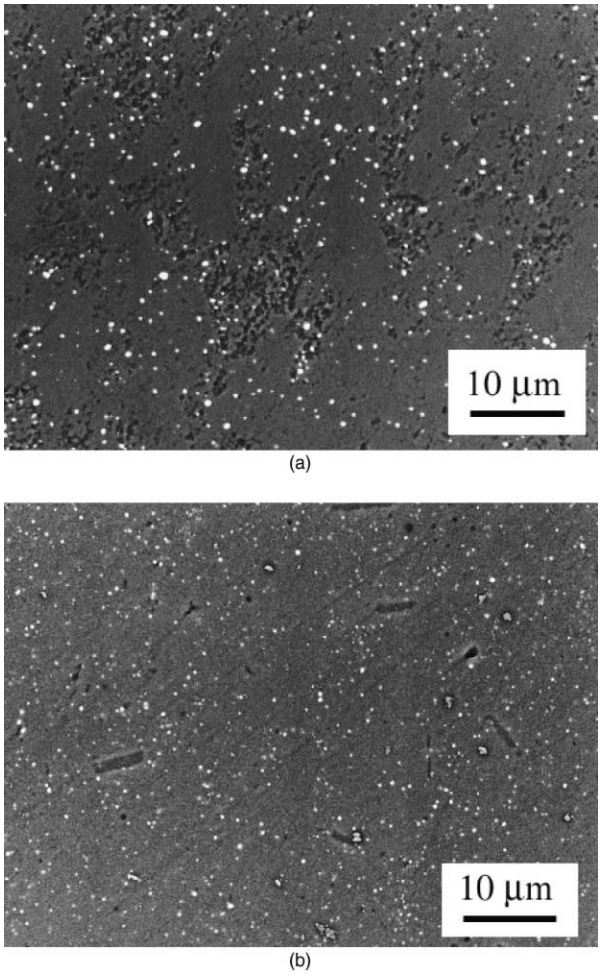

Fig. 4. SEM images of the nanocomposites produced using (a) route I and (b) route II. Note that the composite made using route II is more dense and has a more homogeneous microstructure.

(TD) is achieved by hot pressing at 1400 °C for 30 min. With increasing hot pressing temperature, the density of the alumina increases slightly. Nearly full density was obtained at 1500 °C for 30 min hot pressing. In the case of the Al_2O_3–Cr nanocomposites, the density increased with hot pressing temperature and time, with the highest density, 98.1% TD, achieved by hot pressing at 1600 °C for 60 min. It is assumed that the density would be further improved with higher hot pressing temperatures. However, no attempts to hot press the nanocomposites at temperatures higher than 1600 °C were conducted because the chromium particles would grow too quickly at higher temperatures. Further, the density of Cr_2O_3 (5.21 mg m^{-3}) is lower than that of metal Cr (7.19 mg m^{-3}), which may also partially account for the relatively low density of the nanocomposites.

Reduction of the densification rate by the presence of inert second phase inclusions is well documented. When the second phase particles become much smaller than the matrix grain size, a large number of particles are present per grain facet. Thus, even low volume fractions of second phase have a significant effect on the densification behaviour of nanocomposites, such as Al_2O_3–SiC.[25,26] As chromium is a high melting point metal (1875 °C), it is most likely to be in the solid state in the hot pressing temperature range adopted in this study, i.e. from 1400 to 1600 °C. The presence of solid-state chromium particles at the interfaces may reduce the densification rate. Also, further decomposition of the chromium precursor may also influence the densification behaviour of the Al_2O_3–Cr nanocomposites by forming gaseous products (such as CO) during the sintering process. Further microstructural investigation is necessary to clarify some of these issues.

The thermally etched surfaces of nanocomposites hot pressed at different temperatures, together with those of monolithic alumina, are shown in Fig. 6. The average grain size values of nanocomposites are listed in Table 1. It can be seen that adding 5 vol.% nano-sized chromium significantly decreased the alumina grain size. The

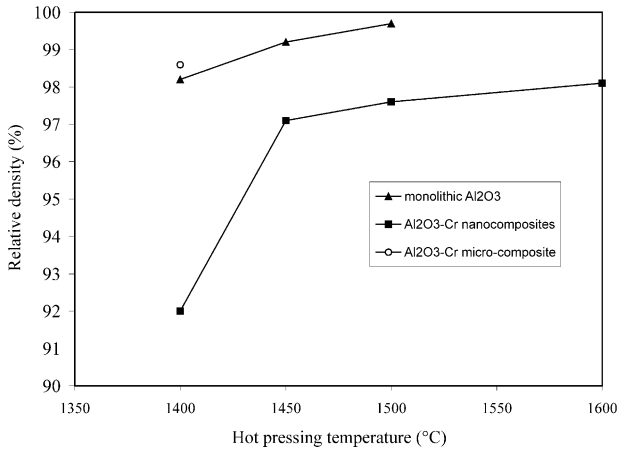

Fig. 5. Relative density as a function of processing temperature for Al_2O_3 and the Al_2O_3–Cr composites.

refinement of microstructure by adding nano-sized Cr inclusions is seen by comparing the grain size of the monolithic alumina (3.5 μm) and the Al_2O_3–Cr nanocomposite (0.68 μm) sintered under identical conditions. Clearly, micrometre sized chromium inclusions do not inhibit grain growth to the same extent as the alumina hot pressed at 1400 °C has a grain size (2.7 μm) that is similar to the Al_2O_3–Cr microcomposite (2.1 μm).

The majority of the alumina grains in the nanocomposite hot pressed at 1450 C are equiaxed and have a narrow size distribution (Fig. 7). Occasionally, alumina grains with higher aspect ratios could be seen. Chromium particles are spherical and homogeneously distributed in the alumina matrix. No obvious glassy phase was present. It is very common to observe strain fringes around nano-sized chromium particles, most likely resulting from stresses arising from a mismatch in the coefficients of thermal expansion of alumina and chromium. Dislocations associated with chromium particles are also observed.

Increasing the hot pressing temperature to 1600 °C caused both the grain size and the particle size to increase (Fig. 8). The average grain size increased to 1.6 μm. Moreover, elongated alumina grains were present. An example of such a high aspect ratio alumina grain is shown in Fig. 9. The facet planes are identified as {0001}. There is some evidence that a glassy phase exists, mainly at the triple points around the chromium particles, and that these areas were associated with higher porosity.

Al_2O_3 abnormal grain growth has been found in Al_2O_3–SiC nanocomposites at fairly high processing temperatures.[27–29] Generally, this was a result of impurities in the powder. Locally high concentrations of some elements, such as Si, Ca and Na, produce a liquid phase during sintering. The mobility of boundaries containing silicate-based liquid films has been demonstrated to be less than clean grain boundaries.[30] It has been shown that the basal planes {0001} are readily wet by the liquid and form the long facets of high aspect ratio during the sintering of alumina.[31] Thus this mobility difference between the interfaces results in the large aspect ratio grains.

Considering the Al_2O_3–Cr nanocomposite hot pressed at 1600 °C, wavelength dispersive X-ray analysis in the SEM suggests that higher concentrations of Na and Ca are present in the lath-like Al_2O_3 grains than in the Al_2O_3 matrix although SADP analysis confirms that both types of grains are α-Al_2O_3. Sodium and calcium are both impurities from the alumina powder. Thus, it appears that at the higher processing temperature, the impurity content of the initial starting powder blend leads to the formation of a small amount of liquid phase which in turn results in the large, lath-like grains in the final microstructure.

The particle size distributions of the chromium in the nanocomposites hot pressed at 1450 and 1600 °C were analysed using TEM images of over 300 particles in each case. The dispersed chromium particles are mostly located at the grain boundaries and triple points. For the Al_2O_3–Cr nanocomposite hot pressed at 1450 °C, 70% (in number) of the chromium particles are located on grain boundaries or at triple points with a mean size of 144 nm, whereas 30% of the chromium particles are trapped inside the alumina grains with a smaller mean particle size of 75 nm. Overall, the mean chromium particle size is 124 nm. After increasing the hot pressing temperature to 1600 °C, the particle sizes at the intragranular and intergranular positions increase to 124 and 213 nm, respectively. The mean particle size is 186 nm. The ratio of inter/intragranular particles is unchanged, although it was noticed that the chromium particles that were trapped inside the elongated alumina grains tended to be bigger than those in the other grains. The nanocomposite fabricated at the lower temperature has a narrower particle size distribution. Some fairly large particles, around 1 μm, can be found in the high temperature sintered compact.

3.3. Mechanical properties

The mechanical properties of Al_2O_3–5% Cr nanocomposites with different hot pressing temperatures, as well as the values of parent alumina specimens and the Al_2O_3–Cr micro-composite, are summarised in Table 2. The detrimental effect of inhomogeneously distributed Cr and low density, as in the material made by powder processing route I, is reflected in the low mechanical properties. It is clear that the influence of processing on the mechanical properties is significant. It is noted that as long as the Al_2O_3 grain size is small (i.e. samples hot pressed at 1450 and 1500 °C) the indentation hardness values of the nanocomposites are similar to the hot pressed monolithic Al_2O_3. Adding nano-sized chromium particles also increased the fracture strength of

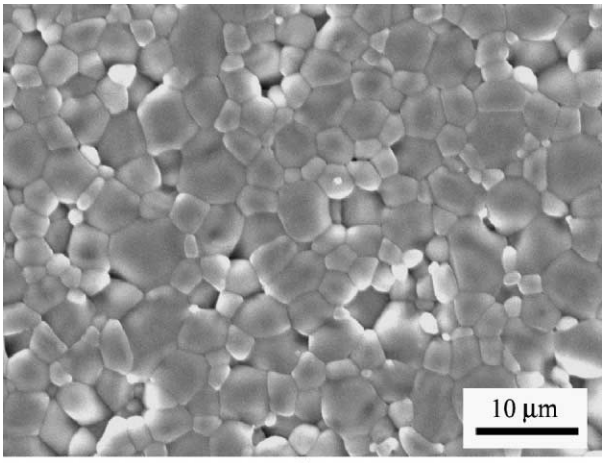

Fig. 6. SEM images of thermally etched surfaces of (a) monolithic alumina hot pressed at 1400 °C for 30 min and (b) nanocomposite hot pressed at 1450 °C for 60 min.

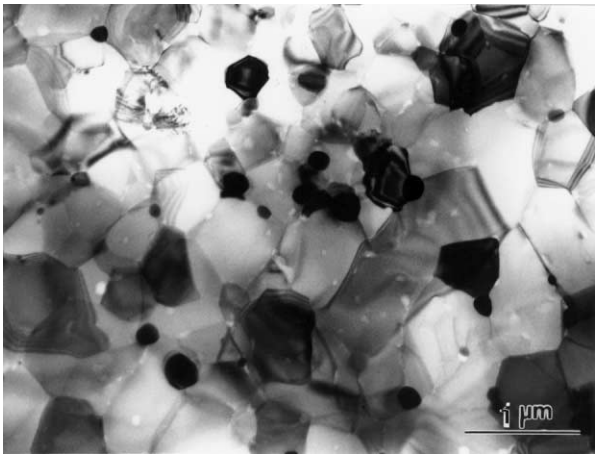

Fig. 7. TEM image showing the fine, equiaxed matrix microstucture of the nanocomposite hot pressed at 1450 °C for 60 min.

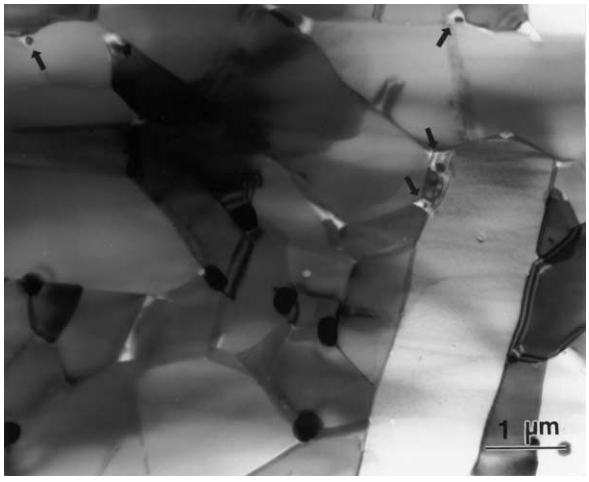

Fig. 8. TEM image of the microstructure of the nanocomposite hot pressed at 1600 °C for 60 min. The arrows indicate positions where a glassy phase may have formed.

the nanocomposites but the fracture toughness either remained unchanged or possibly increased very slightly. The strength of the 5 vol.% Cr–Al_2O_3 microcomposite was comparable to those of the monolithic aluminas. The highest strength and fracture toughness, 736±29 MPa and 4±0.2 MPa $m^{1/2}$, were obtained for the nanocomposite hot pressed at 1450 °C. These values are broadly consistent, in percentage terms, with other hot pressed 5 vol% metal–alumina nanocomposites produced from nitrate precursors, for which strength increases of 35% for pressureless sintered Ni–Al_2O_3,[10] 56% for hot pressed Ni–Al_2O_3[9] and 78% for hot pressed Cu–Al_2O_3[22] have been reported. For the hot pressed composites the actual values of strength were higher than reported here, although the grain size of the alumina matrix, the metal particle size and the fraction of intergranular metallic particles were all comparable. Reported values of the fracture toughness of 5 vol.% metal nanocomposites are slightly higher than the values reported here, being in the range 4.2–4.8 MPa $m^{1/2}$, indicating small improvements over the monolithic alumina value of 3.5 MPa $m^{1/2}$.

In order to investigate the true effect of nano-sized particles on the mechanical properties, the comparison should be based on microstructures with the same density and grain size. It was not possible to produce pure alumina with a grain size as small as that found in the nanocomposites. Fracture strength improvements can result from increases in fracture toughness and/or flaw size reductions. In the case of the Al_2O_3–Cr nanocomposites in this study, the fracture toughness increments are negligible. Thus, it is reasonable to assume that a reduction in the flaw size is responsible for the strengthening. In general, flaw size is related to grain size in dense polycrystalline materials. Therefore, the strength should increase with decreasing grain size. Fig. 10 shows the strength of the hot pressed Al_2O_3 and Al_2O_3–Cr nanocomposites as a function of alumina

grain size. A linear relationship is evident. Thus, the improvement in the fracture strength is a consequence of the microstructure refinement resulting from the addition of nano-sized chromium particles.

It is well known that the most effective toughening mechanism that can be achieved through the addition of metallic inclusions is that of crack bridging. As illustrated in Fig. 11 the indentation introduced cracks are straight and travel along the interface between the Al_2O_3 and the nano-sized chromium particles without any obvious deflection. Cracks are rarely bridged by chromium particles. Therefore, the contribution to toughening from the ductile fracture of chromium is small, especially when the particles are small and spherical. Furthermore, the alumina matrix is likely to have tensile hoop stresses around the chromium particles as a result of the coefficient of thermal expansion of chromium being smaller than that of Al_2O_3 (assuming that the stress due to the mismatch is not relieved entirely by the deformation of the chromium). Crack propagation through a tensile stress region would be promoted and hence is detrimental to toughening. However, the indentation fracture toughness values imply that there should be a toughening mechanism that counteracts this negative factor.

Fracture surfaces of the monolithic Al_2O_3 and the Al_2O_3–Cr nanocomposites exhibit different features as shown in Fig. 12(a) and (b), respectively. The fracture of monolithic alumina is mainly intergranular, although some of the slightly bigger alumina grains show transgranular fracture. Adding 5 vol.% nano-sized chromium changes the fracture mode to transgranular failure. It is difficult to see any plastically deformed chromium particles on the fracture surface of the nanocomposites. Sometimes spherical, slightly bigger chromium particles, usually sitting at grain boundaries, protruding from the fracture surface can be seen. The fracture mode change is also a feature of the extensively investigated Al_2O_3–SiC nanocomposites. The thermal mismatch between chromium and Al_2O_3 is comparable with that between Al_2O_3 and SiC. The high tensile hoop stress developed around intragranular chromium or SiC particles during cooling down from the processing temperature could lead to the crack being attracted into the alumina grains.

The elongated alumina grains in the nanocomposite sintered at 1600 °C could increase the fracture toughness by causing deflection or crack bridging. Bridging of

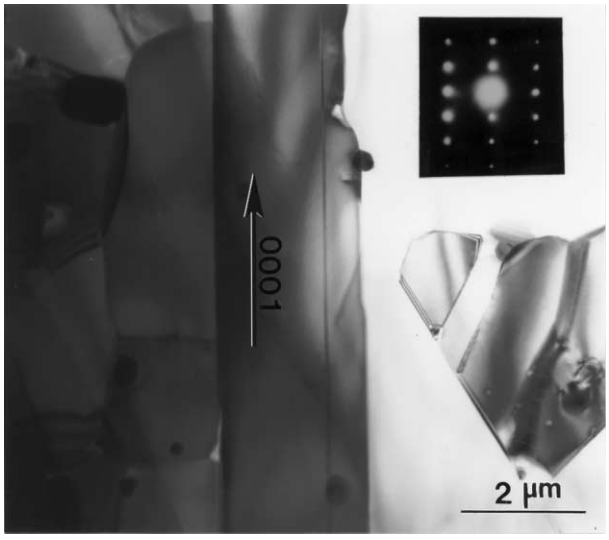

Fig. 9. TEM image and associated SADP of a high aspect ratio alumina grain in the nanocomposite hot pressed at 1600 °C for 60 min.

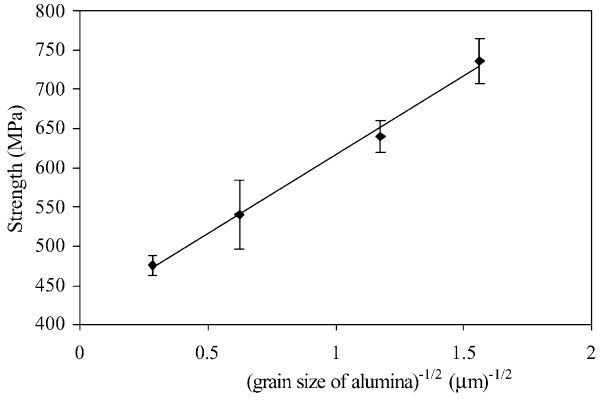

Fig. 10. Strength as a function of grain size for the monolithic alumina and the nanocomposites.

Table 2
Mechanical properties of the hot pressed monolithic Al_2O_3, the Al_2O_3– 5% Cr nano composites and the Al_2O_3–5 vol.% Cr microcomposite

	Specimen	Indentation toughness (MPa $m^{1/2}$)	Hardness (MPa)	Strength (MPa)
Hot pressed, 1400 °C	Al_2O_3	3.6±0.2	17.6±0.3	425±86
Hot pressed, 1450 °C	Al_2O_3	3.6±0.2	17.2±0.4	475±12
Nano, Route I	Al_2O_3–Cr	3.6±0.4	15.5±0.6	447±18
Nano, Route II	Al_2O_3–Cr	4.0±0.2	17.9±0.5	736±29
Nano, Route II	Al_2O_3–Cr	3.8±0.3	17.7±0.3	640±20
Nano, Route II	Al_2O_3–Cr	3.8±0.2	16.8±0.5	540±44
Micro	Al_2O_3–Cr	3.8±0.2	16.1±0.6	457±12

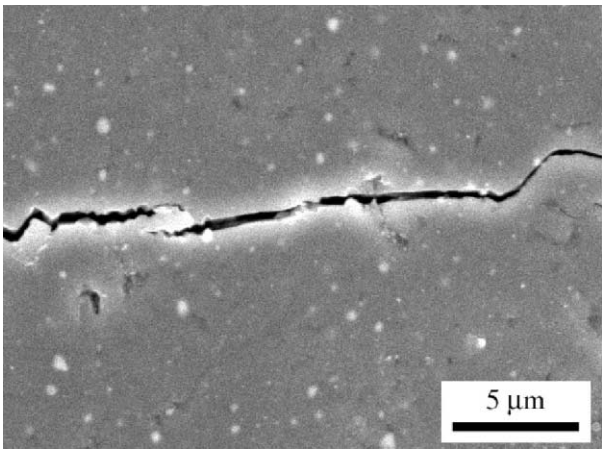

Fig. 11. SEM image of a radial indentation crack in a nanocomposite.

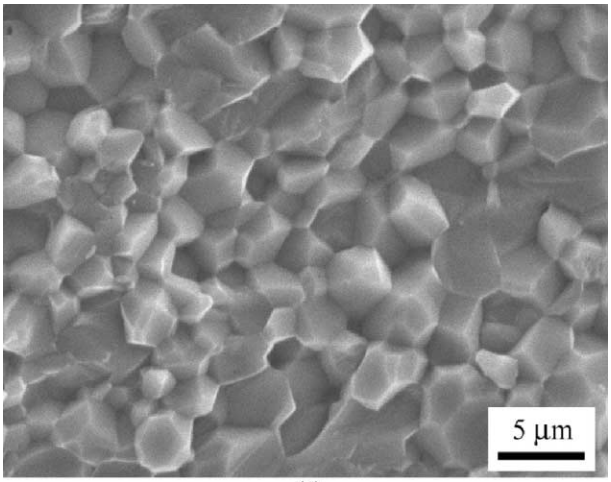

(a)

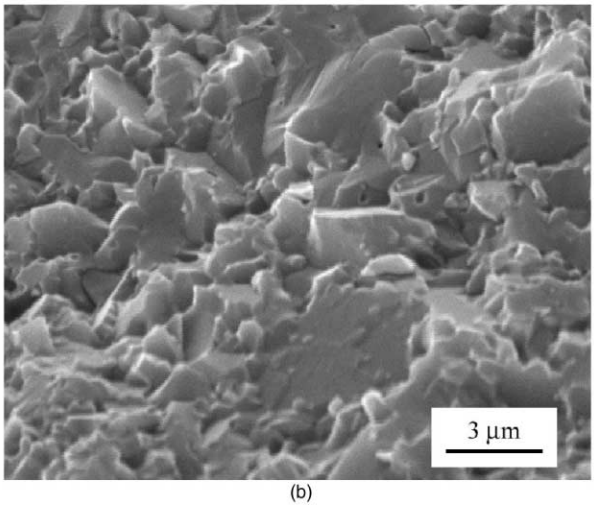

(b)

Fig. 12. SEM images of fracture surfaces of (a) monolithic alumina and (b) a nanocomposite hot pressed at 1450 °C for 60 min.

a propagating crack by Al_2O_3 was found at some positions. However, the indentation fracture toughness was not improved for the higher temperature sintered nanocomposite. Rather, it decreased with increasing hot pressing temperature. The formation of a glassy phase may have weakened the interfaces and provided a preferential crack path. Further, it was found that with increasing hot pressing temperature, the tendency to intergranular failure increased. As the ratio of intragranular to intergranular particles is not changed with increasing hot pressing temperature, intergranular failure most likely results from the interfacial weakness. This may also account for the slight decrease in fracture toughness of the Al_2O_3–Cr nanocomposites fabricated at the higher temperatures.

4. Conclusions

Al_2O_3–Cr nanocomposites have been fabricated using a chemical method with $Cr(ACAC)_3$ as the Cr precursor. Adding 5 vol.% nano-sized chromium particles decreased the densification rate of the alumina matrix. The Al_2O_3–Cr nanocomposite hot pressed at 1450 °C showed a homogeneous distribution of alumina grains and chromium particles and the mean grain size was reduced dramatically to 0.68 μm compared with a grain size of 3.6 μm in the monolithic alumina hot pressed under identical conditions. Increasing the hot pressing temperature caused both grain sizes and particle sizes to increase. Moreover, some alumina grains grew abnormally to high aspect ratio. This may be caused by local liquid phase formation from the impurity elements in the starting powder and powder processing.

The details of the processing procedure are crucial in determining the mechanical properties of the Al_2O_3–5% Cr nanocomposites. The highest strength and fracture toughness, 736 ± 29 MPa and 4.0 ± 0.2 MPa $m^{1/2}$, respectively, were obtained for the nanocomposite hot pressed at 1450 °C. It has been shown that the strengthening in Al_2O_3–5% Cr nanocomposites mainly results from microstructure refinement by adding homogeneously distributed, nano-sized Cr inclusions. Crack bridging and crack deflection by the nano-sized Cr particles did not occur to any significant extent. A fracture mode change from intergranular fracture for monolithic alumina to transgranular failure for the nanocomposites was observed and may account for the slight increase in fracture toughness.

Acknowledgements

We are grateful to the former School of Mechanical and Materials Engineering at the University of Surrey for providing a scholarship for Ying Ji.

References

1. Breval, E., Deng, Z., Chiou, S. and Pantano, C. G., Sol-gel prepared Ni-alumina composite materials: part 1 microstructure and mechanical properties. *J. Mater. Sci.*, 1992, **27**, 1464–1468.
2. Breval, E. and Pantano, C. G., Sol-gel prepared Ni-alumina composites materials: part 2 structure and hot-pressing temperature. *J. Mater. Sci.*, 1992, **27**, 5463–5469.
3. Tuan, W. H. and Brook, R. J., The toughening of alumina with nickel inclusion. *J. Eur. Ceram. Soc.*, 1990, **6**, 31–37.
4. Sun, X. and Yeomans, J., Optimization of a ductile-particle-toughened ceramic. *J. Am. Ceram. Soc.*, 1996, **79**, 2705–2717.
5. Trusty, P. A. and Yeomans, J. A., The toughening of alumina with iron: effects of iron distribution on fracture toughness. *J. Eur. Ceram. Soc.*, 1998, **18**, 495–504.
6. Chou, W. B. and Tuan, W. H., Toughening and strengthening with silver inclusions. *J. Eur. Ceram. Soc.*, 1995, **15**, 291–295.
7. Sbaizero, O. and Pezzotti, G., Influence of residual and bridging stress on the R-curve behaviour of Mo- and FeAl-toughened alumina. *J. Eur. Ceram. Soc.*, 2000, **20**, 1145–1152.
8. Niihara, K., New design concept of structural ceramic–ceramic nanocomposites. *J. Ceram. Soc. Jpn.*, 1991, **99**, 974–982.
9. Sekino, T., Nakajima, T., Ueda, S. and Niihara, K., Reduction and sintering of a nickel-dispersed-alumina composite and its properties. *J. Am. Ceram. Soc.*, 1997, **80**, 1139–1148.
10. Chen, R. Z. and Tuan, W. H., Pressureless sintering of Al_2O_3/Ni nanocomposites. *J. Eur. Ceram. Soc.*, 1999, **19**, 463–468.
11. Nawa, M., Sekino, T. and Niihara, K., Fabrication and mechanical behaviour of Al_2O_3/Mo nanocomposites. *J. Mater. Sci.*, 1994, **29**, 3185–3192.
12. Sekino, T. and Niihara, K., Microstructural characteristics and mechanical properties for Al_2O_3/metal nanocomposites. *Nanostruct. Mater.*, 1995, **6**, 663–666.
13. Sekino, T. and Niihara, K., Fabrication and mechanical properties of fine tungsten-dispersed alumina-based composites. *J. Mater. Sci.*, 1997, **32**, 3943–3949.
14. Guichard, J. L., Tillement, O. and Mocellin, A., Preparation and characterization of alumina-iron cermets by hot pressing nanocomposite powders. *J. Mater. Sci.*, 1997, **32**, 4513–4521.
15. Guichard, J. L., Tillement, O. and Mocellin, A., Alumina-chromium cermets by hot-pressing of nanocomposite powders. *J. Eur. Ceram. Soc.*, 1998, **18**, 1743.
16. Oh, S.-T., Sekino, T. and Niihara, K., Fabrication and mechanical properties of 5 vol.% copper dispersed alumina nanocomposite. *J. Eur. Ceram. Soc.*, 1998, **18**, 31–37.
17. Oh, S-T., Sand, M. and Niihara, K., Preparation and properties of alumina/nickel-cobalt alloy nanocomposites. *J. Am. Ceram. Soc.*, 1998, **81**, 3013–3015.
18. Laurent, Ch., Peigney, A., Quénard, O. and Rousset, A., Synthesis and mechanical properties of nanometric metal particles-ceramic matrix nanocomposites. *Sil. Ind.*, 1998, **63**, 77–84.
19. Lu, J., Gao, L., Guo, J. and Niihara, K., Preparation, sintering behavior, and microstructural studies of Al_2O_3/Mo composites from boehmite-coated Mo powders. *Mater. Res. Bull.*, 2000, **35**, 2387–2396.
20. Lu, J., Gao, L., Sun, J., Gui, L. and Guo, J., Effect of nickel content on the sintering behavior, mechanical and electrical properties of Al_2O_3/Ni composites from coated powders. *Mater. Sci. Eng.*, 2000, **A293**, 223–228.
21. Lieberthal, M. and Kaplan, W. D., Processing and properties of Al_2O_3 nanocomposites reinforced with sub-micron Ni and $NiAl_2O_4$. *Mater. Sci. Eng.*, 2001, **A302**, 83–91.
22. Oh, S-T., Lee, J-S., Sekino, T. and Niihara, K., Fabrication of Cu dispersed Al_2O_3 nanocomposites using Al_2O_3/CuO and Al_2O_3/Cu-nitrate mixtures. *Scripta Mater.*, 2001, **44**, 2117–2120.
23. Oh, S-T., Sando, M. and Niihara, K., Processing and properties of Ni-Co alloy dispersed Al_2O_3 nanocomposites. *Scripta Mater.*, 1998, **39**, 1413–1418.
24. Liang, K. M., Orange, G. and Fantozzi, G., Evaluation of indentation fracture toughness of ceramic materials. *J. Mater. Sci.*, 1990, **25**, 207–214.
25. Nakahira, A. and Niihara, K., Sintering behaviors and consolidation process for Al_2O_3/SiC nanocomposites. *J. Ceram. Soc. Japan*, 1992, **100**, 448–453.
26. Stearns, L. C., Zhao, J. and Harmer, M. P., Processing and microstructure development in Al_2O_3-SiC 'nanocomposites'. *J. Eur. Ceram. Soc.*, 1992, **10**, 473–477.
27. Zhang, Y., Deng, Z., Shi, J., Mao, Y. and Guo, J., Microstructure and mechanical properties of SiC particle reinforced Al_2O_3 matrix composites. *J. Mater. Sci. Lett.*, 1996, **15**, 1927–1931.
28. Jeong, Y. K., Nakahira, A., Morgan, P. E. D. and Niihara, K., Effect of milling conditions on the strength of alumina–silicon carbide nanocomposites. *J. Am. Ceram. Soc.*, 1997, **80**, 1307–1309.
29. Borsa, C. E., Ferreira, H. S. and Kiminami, R. H. G. A., Liquid phase sintering of Al_2O_3/SiC nanocomposites. *J. Eur. Ceram. Soc.*, 1999, **19**, 615–621.
30. Kaysser, W. A., Sprossler, M., Handwerker, C. A. and Blendell, J. E., Effect of a liquid phase on the morphology of grain growth in alumina. *J. Am. Ceram. Soc.*, 1987, **70**, 339–343.
31. Bateman, C. A., Bennison, S. J. and Harmer, M. P., Mechanism for the role of magnesia in the sintering of alumina containing small amount of a liquid phase. *J. Am. Ceram. Soc.*, 1989, **72**, 1241–1244.